

High Signal-to-Noise, Differential NICMOS Spectrophotometry

R.L. Gilliland, S. Arribas
January 7, 2003

ABSTRACT

We report analysis for NICMOS CAL/9642, High S/N Capability Characterization. The purpose of this three orbit test was to establish NICMOS time domain stability in a domain not previously tested for NICMOS. Observations of the bright ($H = 6.13$) G0 V star HD 209458 were obtained using 1.8 second MULTIACCUMs with G141 on NIC3. Exposure-to-exposure stability summed over the full spectrum provides S/N of 2000, i.e. we demonstrated 0.5 mmag photometric precision treating the observations simply as broad-band, time-series photometry. Orbit-to-orbit means in a 0.2 micron band taken in ratio to neighboring continuum, without applying any corrections for correlated variations in contemporaneous auxiliary parameters, differed by only 3×10^{-4} . A much better result was obtained with application of such corrections, but the result cannot be considered secure with comparison of only two orbits data. There is an excellent chance that in applications with sufficient flux to generate the required Poisson limit, that well planned NICMOS observations can provide differential spectrophotometric stability better than 1 part in 10,000 if not even significantly better.

Introduction

Some science applications require extremely high S/N measurements, usually in a form where only differential changes over time are tracked. For example with STIS we know that by using the gratings to disperse light over a large number of pixels, time-series S/N ~

High Signal-to-Noise, Differential NICMOS Spectrophotometry

10,000 per readout is possible from summing over all of the illuminated pixels. Furthermore, the spectral stability inherent in the STIS exposures is such that near Poisson limited results can be obtained for differential spectrophotometry. The steps to demonstrating such stability for CCDs in general has involved both laboratory investigations (e.g. Robinson et al. 1995), and for STIS in particular on-orbit testing (Gilliland, Goudfrooij, and Kimble 1999; Gilliland 1999).

In principle the stable environment provided by HST and NICMOS, especially in the NCS era, may facilitate achieving ultra-high S/N results as have been found to hold for CCDs. There are a number of challenges facing such observations with NICMOS. Reaching high S/N of 10,000 requires of course that at least 10^8 photons be recorded in the interval of interest, and that no sources of systematic or other random noise degrade the results beyond the desired limit. Since the full well depth of NICMOS is $\sim 10^5$ electrons, and in normal imaging mode much of the flux falls on the central pixel, it is necessary to either sum over hundreds of individual observations (not practical given the time overheads associated with NICMOS exposures), or to take advantage of spreading the image over many pixels. Since NICMOS has a grism capability, and it has an internal focus mechanism it is possible to obtain high count rates taking advantage of both spectroscopy and a moderate degree of image defocus. Particular limitations that might apply for NIC3 observations with a grism include: (1) The NIC3 pixels severely undersample the intermediate wavelengths, and intra-pixel quantum efficiency variations of 20-30% strongly couple small guiding errors to changes of count rate. (2) The NICMOS detectors have a quantum efficiency that is sensitive to temperature fluctuations. This is exacerbated by not having a robust measure of NIC3 temperature available from telemetry, but improved generally in the NCS era by excellent stability. (3) The NICMOS detectors exhibit significant nonlinearity at high count levels. The interaction of one, or more of these limitations coupled with either temperature fluctuations, and/or guiding errors could easily dominate the error budget limiting S/N to values well under the Poisson limit, unless these can be controlled for in either observation planning or subsequent data analysis.

For this characterization experiment we explored the possibility of trailing the telescope along the cross-dispersion direction over some 20 arcsec (100 pixels) for one minute exposures. This would allow averaging the signal over a large number of subpixel positions (helping with the intra-pixel QE problem), while allowing for a very high effective count rate. Unfortunately, this approach proved to be infeasible at the Phase II level now that telescope SCANS are no longer available.

Observations

Since the capability to be tested is motivated by science possibilities related to the detection of atmospheric constituents of planets that can be probed by comparing in-transit to out-of-transit spectrophotometry (e.g. as with STIS: Charbonneau, D. et al. 2002), we chose HD 209458 as the star for these observations. As a test of stability, and to avoid mixing science with calibration, these three consecutive orbits of observation were restricted to fall well outside of planet transit or eclipse times. As executed the observations started about 4 hours after the egress of an HD 209458b transit.

These CAL/9642 observations were executed December 10, 2002 and are of course in the public domain. The lead author can be contacted (for the next year) for intermediate data products related to these tests if the reader is interested in extending these results.

A PAM defocus to -0.5 mm (as in CAL/9323) was adopted to provide a FWHM for NIC3 of about 5 pixels. The resulting spectral resolution will be 30 -- 50 as compared to the standard 100 for NICMOS spectroscopy. The defocus accomplishes two things for our purposes: (1) The intra-pixel sensitivity variations with NIC3 are effectively averaged over making the resulting integrated counts less sensitive to the inevitable small guiding errors. (2) Allows longer integration times to be adopted before nearing the full well depth limit of the detectors. Even with this defocus, the integration time to reach the goal of half of full well depth on the brightest pixels was reached in a little under 2 seconds.

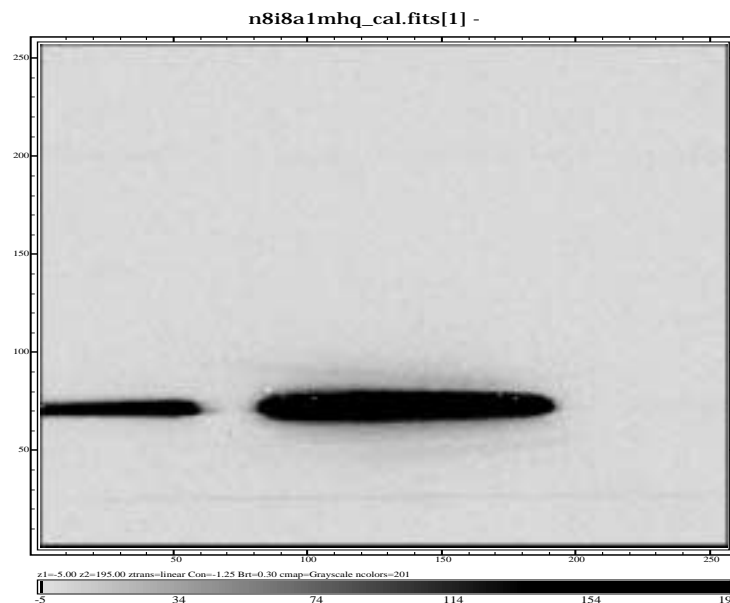


Figure 1- A single (of 392 taken) MULTIACCUM exposure of 1.8 s with NICMOS. The first order spectrum is centered on rows 69-70 and extends from column 75 (2.0 microns) to 200 (1.0 microns).

High Signal-to-Noise, Differential NICMOS Spectrophotometry

We chose the MCAMRR MULTIACCUM with NSAMP=6 providing 1.814 s effective integrations. In orbits after the first (which included time for PAM defocus) it was possible to obtain a total of 136 such exposures for a total of 246.7 seconds of actual exposure time per orbit. Thus, for this bright star the instrument overheads limit the effective duty cycle to only about 10% even with the coupled use of defocus and spectroscopy. The resulting detected photon level exceeds 10^8 for the sum of 4 consecutive exposures (summed over wavelength and cross dispersion), thus providing 34 measures with a Poisson limit of 10,000 each per HST orbit.

In order to assess sensitivity to small guiding errors the observations within each orbit are taken in 4 blocks, the first and last at the nominal pointing zero, with the central two blocks dithered in cross-dispersion by +/- 0.1 pixels. Sequences within orbits for these primary exposures were kept as uniform as possible.

In the last orbit a direct image with a narrow-band filter was taken to establish the pointing as required to determine wavelengths for the grism spectra. Also exposures with the other two grisms, G096 and G206 were obtained at the end.

For purposes of orientation only a flux calibrated spectrum for one of the 1.8 s G141 exposures of HD 209458 is shown in Figure 2 -- extracted using the NICMOSlook software.

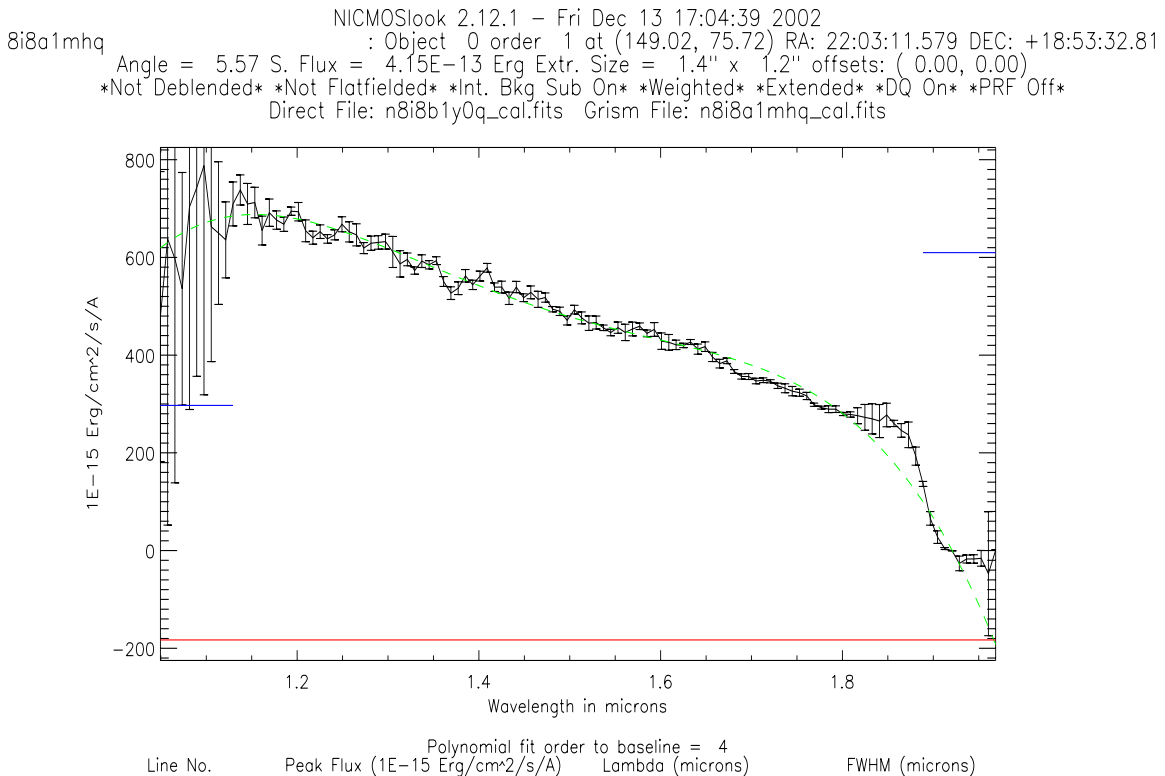


Figure 2-The flux calibrated, extracted spectrum for HD 209458 in G141 using the NICMOSlook software. (Just for illustration, not using this for the time series analysis.)

Data Reductions

Our analyses start with the CAL extension pipeline calibration/reductions for each of the 1.814 second MULTIACCUMS. The pipeline reductions include all of the expected NICMOS steps with the important exception of flat-fielding. The latter is not performed in the pipeline, since the grism spectroscopy requires generation of scene dependent flats that take into account the actual wavelength falling on individual pixels. Although in principle flat-fielding might be considered optional for these observations, since we only care about differential changes in time, application of good flat fields should reduce sensitivity to pixel-to-pixel QE changes interacting with offsets to produce spurious count changes. We therefore adopted the approach recommended in the NICMOS Data Handbook and generated our own wavelength dependent flat field.

To form the wavelength dependent flat we: (1) Established the wavelength for each column in the first order spectrum (e.g. see Figure 1). (2) Used the current NCS on-orbit flats for F108N, F113N, F164N, F166N, F187N, F190N and F196N to fit the wavelength dependence in the flats as a quadratic function over wavelength at each pixel. (3) The resulting quadratic was then evaluated at the appropriate wavelength by column and applied as a multiplicative correction to all pixels in the column to be summed over in the spectral extraction. The quadratic fits for wavelength dependence worked very well with rms residuals usually at the 0.001 level. Outside of the pixel area dominated by the first order stellar spectrum we simply adopted the F160W flat field to represent a wavelength integrated mean.

Application of the derived flat fields for the G141 observations resulted in a total of 392 corrected versions of the .CAL files. Also, at this step the few bad pixels within the domain of the first order spectrum were identified from examination of the data quality array, and data values for these pixels were replaced by linear interpolation over the nearest good pixels. Since none of the bad pixels fell near peak count levels in the first order spectrum this was a benign step that facilitates easy extraction. Finally, the global background value evaluated in a blank part of the images was subtracted from all pixels.

Time Series Extractions and Decorrelation

The next step was to extract one-dimensional spectra for each of these observations while at the same time tracking auxiliary characteristics of the data (e.g. full width half maximum in the cross-dispersion direction, mean location of the spectra in x and y, etc.) For each column within the one dimension spectrum which covers roughly $x = 80,190$ and $y = 60,80$ (see Figure 1) we chose an extraction box that started and stopped at levels where

High Signal-to-Noise, Differential NICMOS Spectrophotometry

the flux was a few times 10^{-3} the central intensity and where the flux had reached a generally flat wing with equal intensity above and below in order to minimize sensitivity in the counts to small guiding errors.

In order to simplify signal-to-noise tracking the one-dimensional spectra were converted to electrons per 1.814 second integration by multiplying by the exposure time, and by the gain of 6.5 electrons per DN.

The auxiliary variables computed for each of the 392 time steps of G141 spectra included:

- 1) The mean width of the spectrum in cross dispersion created by averaging the widths from a Gaussian fit at each column for which the central intensity reached 10,000 electrons.
- 2) The mean position of the spectrum in cross dispersion (y) from averaging the centroids of the Gaussian fits.
- 3) The mean rotation of the first order spectrum evaluated as the mean y-position for the last 10 columns minus the same for the first 10 columns. This was not a variation that had been expected, but inspection of grism images from different orbits suggested that a rotation happened nonetheless. We now believe this results from the filter wheel having been rotated to the blank position for each occultation and not resetting perfectly. Noteworthy here is the uniqueness of orbit 2 -- a rather problematic occurrence since we wish to compare results in orbit-to-orbit means and always suspected that the first orbit might show unique behavior. Thus, each orbit-to-orbit set has some unique behavior evidenced by the auxiliary parameters.
- 4) An overall background mean evaluated well away from the first and second order spectra, and avoiding the electronic ghost of these offset by 128 pixels in y.
- 5) A potential proxy for the detector temperature formed as the difference between means over columns in the background in such a way as to bring out maximum sensitivity to expected temperature dependent shading profiles for NIC3 (see Fig. 7.11 of the NICMOS Instrument Handbook).
- 6) A temperature proxy control chosen as column mean differences in the background that should not show a shading sensitivity for NIC3.

Figure 3 shows an example of the one-dimensional extracted spectra peaking at about 350,000 electrons per column. Total integrated counts are about 2.67×10^7 electrons per

High Signal-to-Noise, Differential NICMOS Spectrophotometry

integration. Two time series quantities will be considered: (1) The direct sum of counts over the full spectrum, i.e. a time-series of broad-band photometry equivalent. (2) A differential spectrophotometric measure formed as the ratio of the central "Band" in Figure 3 ratioed to the sum of the neighboring continuum regions. The spectral structure seen results almost entirely from the grism sensitivity function.

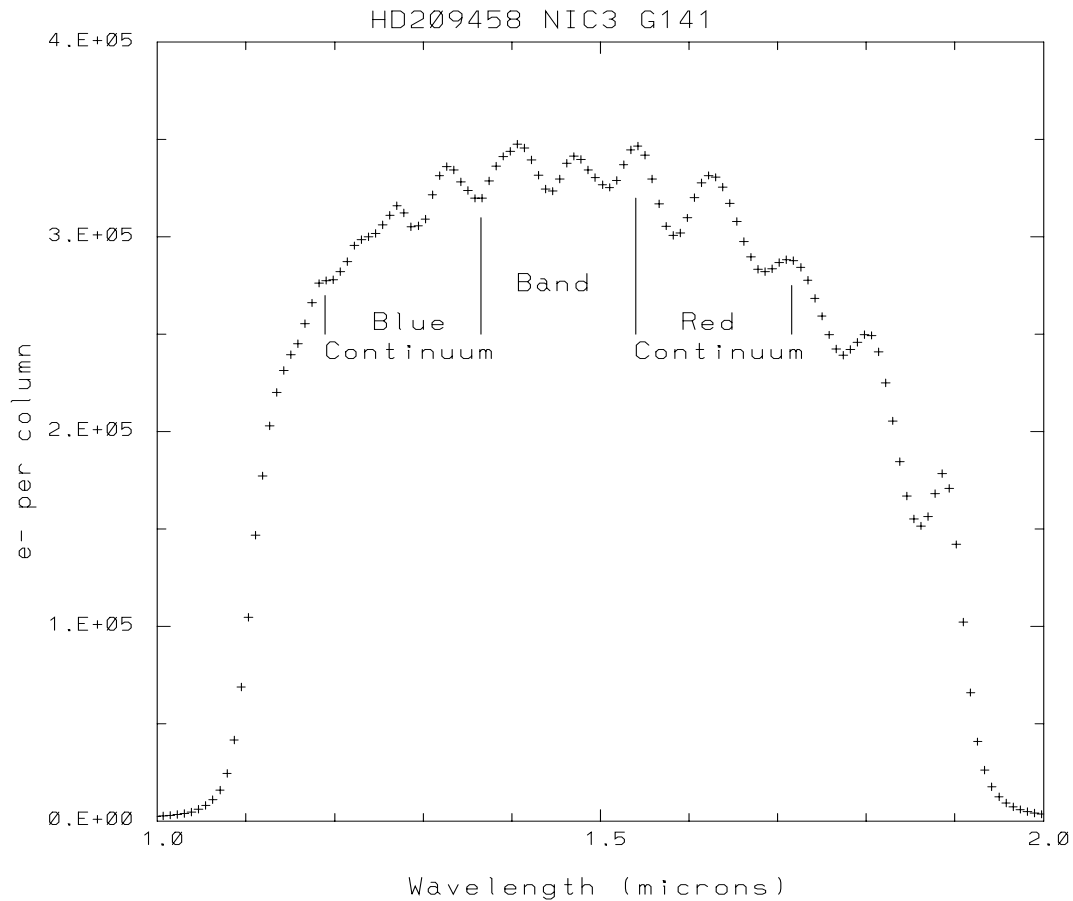


Figure 3 -Electrons per column (sum over some 20 rows) against wavelength in microns for a single 1.8s MULTIACCUM. Bands to be used later in tracking differential spectrophotometry are shown. The spectral features here simply reflect the sensitivity of the grism with wavelength, not real stellar features.

The remaining figures all illustrate aspects of the time series. The direct time series sum over the full spectra is shown in Figure 4 --note that the three orbits are shown by a vertical line separating blocks of points, in actuality a gap of some 50 minutes of course exists between orbits. Several features are obvious from inspection of the direct time series: (1) The initial few points are low in the orbits, particularly pronounced in the first orbit. (2) There is a characteristic offset from the 2nd to 3rd quarters of the data in each orbit, almost

High Signal-to-Noise, Differential NICMOS Spectrophotometry

certainly following from the ± 0.1 pixel cross-dispersion dithers used coupling with residual detector sensitivity. (3) An overall upward trend in time both within orbits and orbit-to-orbit.

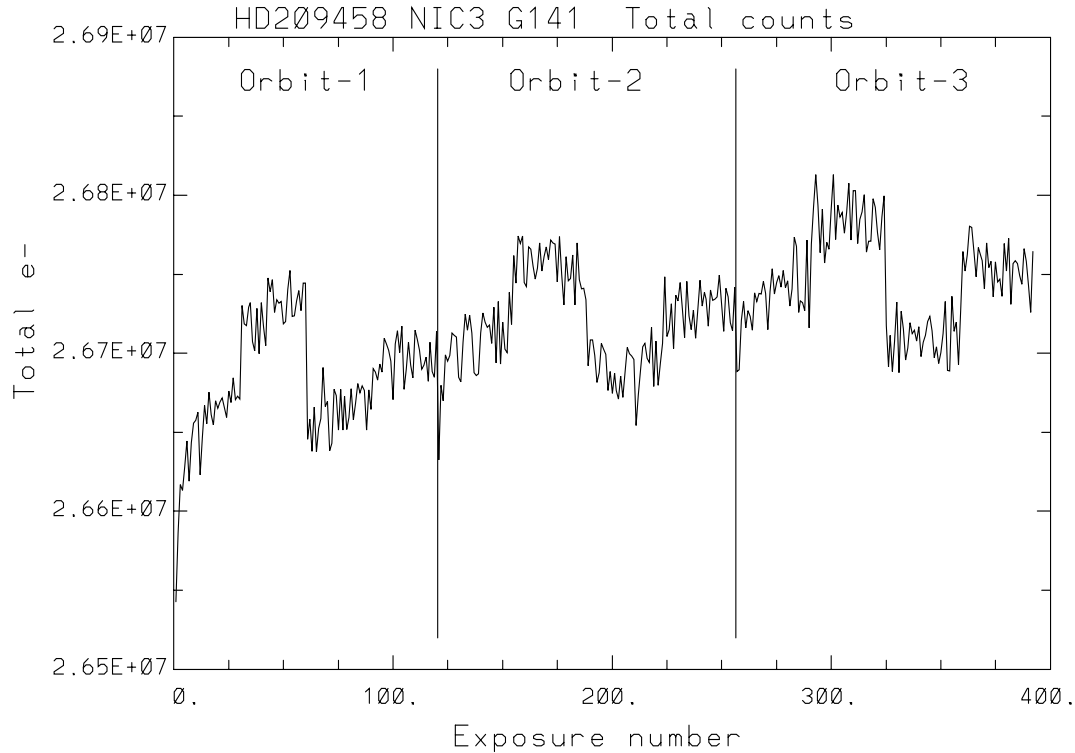


Figure 4- Total electrons detected per MULTIACCUM summed over the full first order spectrum plotted against exposure number in sequence. Vertical lines are drawn at the points separating the three contiguous orbits (gaps of 50 mins in reality at these times, and smaller gaps every 10 or so points at buffer dumps). There were 120 exps in orbit no. 1, 136 each in orbits 2 and 3.

The several auxiliary parameters are shown in Figures 5a and 5b. The panels are defined in the figure captions, here we will offer a few comments on the behavior of each parameter. The mean y-position shows orbit-to-orbit changes at the level of about 0.05 pixels and the most obvious feature follows from the imposed ± 0.1 pixel dithering each orbit. The width of the spectrum in cross dispersion seems to show primarily changes during the course of individual orbits. The order rotation shown in Panel C shows primarily an offset of orbit 2 relative to the other orbits. The mean position of the spectrum in x shows a change primarily between orbits 1 and 2. Panel E shows relative, reconstructed temperatures courtesy of E. Bergeron based on an analysis of the data bias levels that have been shown to correlate tightly with temperature; here the main trend is orbit-to-orbit with slight drifts within orbits. The mean background shown in Panel F appears to be random

High Signal-to-Noise, Differential NICMOS Spectrophotometry

noise, albeit at a level a factor of a few larger than the expected level of Poisson fluctuations here. Panel G shows the temperature proxy based on regions of NIC3 expected to show temperature sensitivity via "shading"; no obvious trends. And finally Panel H is a comparable control as in G, but for regions not expected to reflect temperature differences.

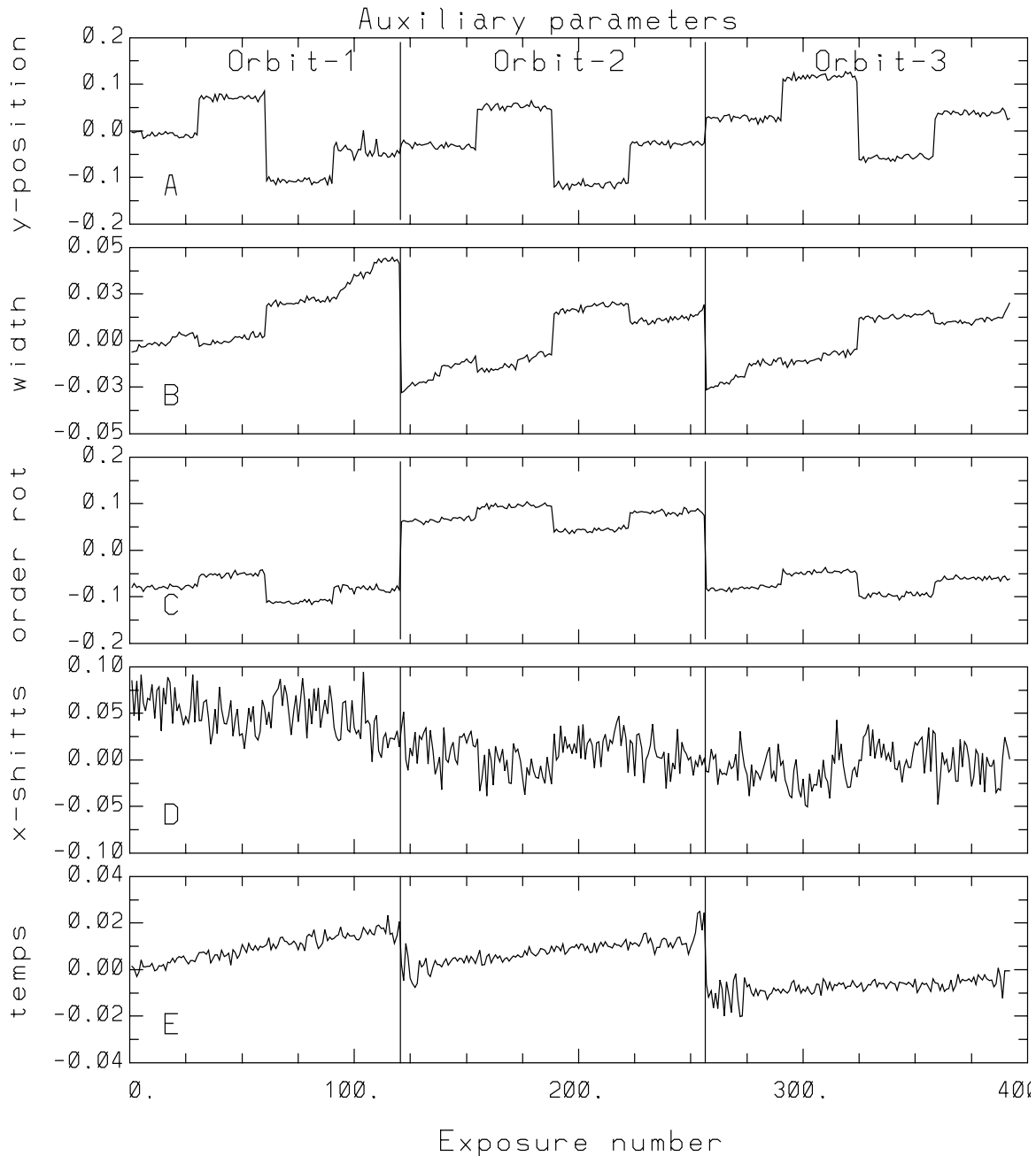


Figure 5a (see caption on next page)

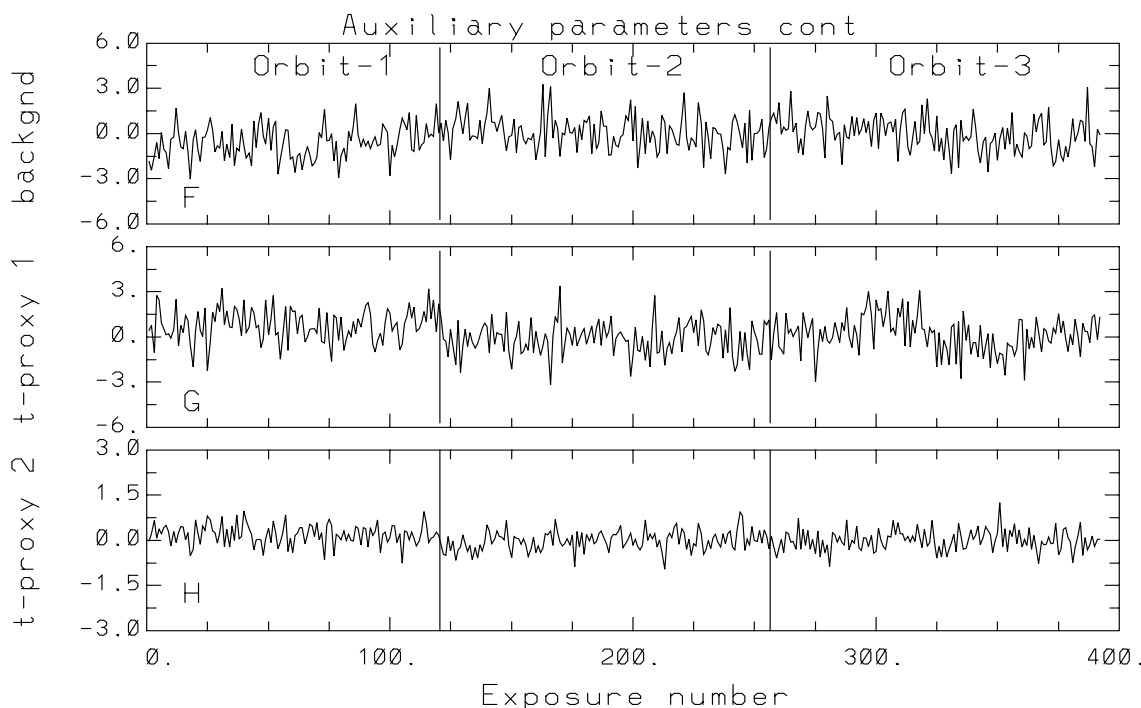


Figure 5a and 5b. Values of several auxiliary parameters (all have been used in decorrelating the intensity time series) associated with the data. Values in parentheses for each give the magnitude of linear correlation with respect to direct and bandpass differential time series respectively. Panels A -- H are:

A. The mean position of the spectrum in the y -direction evaluated from Gaussian fits in cross dispersion at each column with good signal. In order to test sensitivity to small offset each orbit started with a block at nominal position, then dithered the obs by $+0.1$ pixel, then -0.1 , then back to nominal. Anything else is drift or error (0.89, 0.74).

B. Mean cross-dispersion width of the spectrum (0.39, 0.33).

C. Rotation (height near one end minus height at the other end). The variation orbit-to-orbit was not expected. It turns out the system rotates the filter wheel during each occultation, so probably explained by not having returned exactly (0.16, 0.08).

D. Shift along the dispersion evaluated from cross-correlation of extracted spectra (0.54, 0.40).

E. A temperature record evaluated from analysis of the bias level associated with the data (courtesy of E. Bergeron) (0.38, 0.11).

F. Mean background level in e - from well away from the spectrum, this value had already been subtracted at the image level processing (0.10, 0.09).

G. Another Temp proxy based on shape of background (0.28, 0.13).

H. Yet another temp-like proxy, differencing different regions of background not expected to show T dependence (0.01, 0.05).

High Signal-to-Noise, Differential NICMOS Spectrophotometry

The primary analysis now starts with the vector shown in Figure 4, the time series photometry, and decorrelates that with all of the available auxiliary parameters. The result of doing this is shown in Figure 6 where the upper panel merely repeats Figure 4, but now after subtracting the mean and normalizing by the mean -- note that except for the first few points in orbit 1 all of the points stay within a peak-to-peak band of about 0.6%. Given 2.67×10^7 electrons per observation the Poisson limit is about 5,167 per point, taking into account extra noise from the significant 30 electron read noise on the ~ 2000 pixels extracted per spectrum leads to a projected S/N of 5,000 per point for an expected rms of 0.02%. The lower panel of Figure 6 shows the decorrelated result. For this the decorrelation was based on a multi-linear regression with the eight vectors of Figures 5a and 5b using only orbits 2 and 3 in the fit and also ignoring the first and last four points in these orbits. Orbit 1 was included initially, but it was quickly concluded (as turns out to be the case for STIS as well) that the first orbit was showing unique behavior.

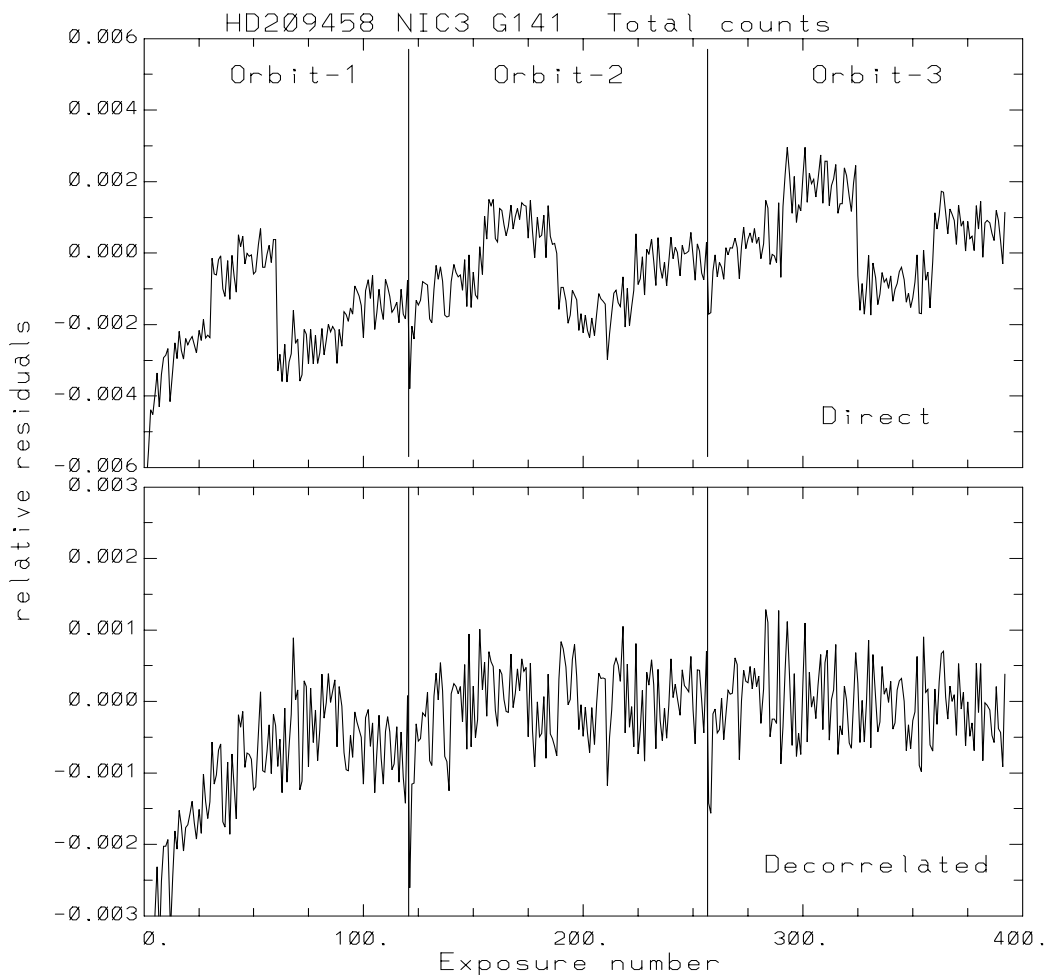


Figure 6- Upper panel (same as Fig.4) shows direct record of total intensity after subtracting the mean and normalizing by the mean. Lower panel shows the same after decorrelating the above by the 8 vectors shown in Figs 5a and 5b. (See text for details.)

High Signal-to-Noise, Differential NICMOS Spectrophotometry

In all that follows we carry orbit 1 in the plots, but use only points in orbits 2 and 3 for numerical results. The point-to-point rms after decorrelation is 0.0005, i.e. a S/N of 2000. This is reasonably impressive for the 1.8 s integrations, but does not reach the Poisson limit more than a factor of two better than this. (Note that if the primary goal here were to study a phenomenon on short timescales, then it would be reasonable to first high-pass filter both the signal and auxiliary parameter vectors before evaluating the multi-linear regression. There is a good chance this would result in a significant gain for high frequency variations.)

Figure 7 shows in the upper panel the direct time series (after removing the mean and normalizing by the mean) for the differential spectrophotometry (central band normalized by neighboring continua).

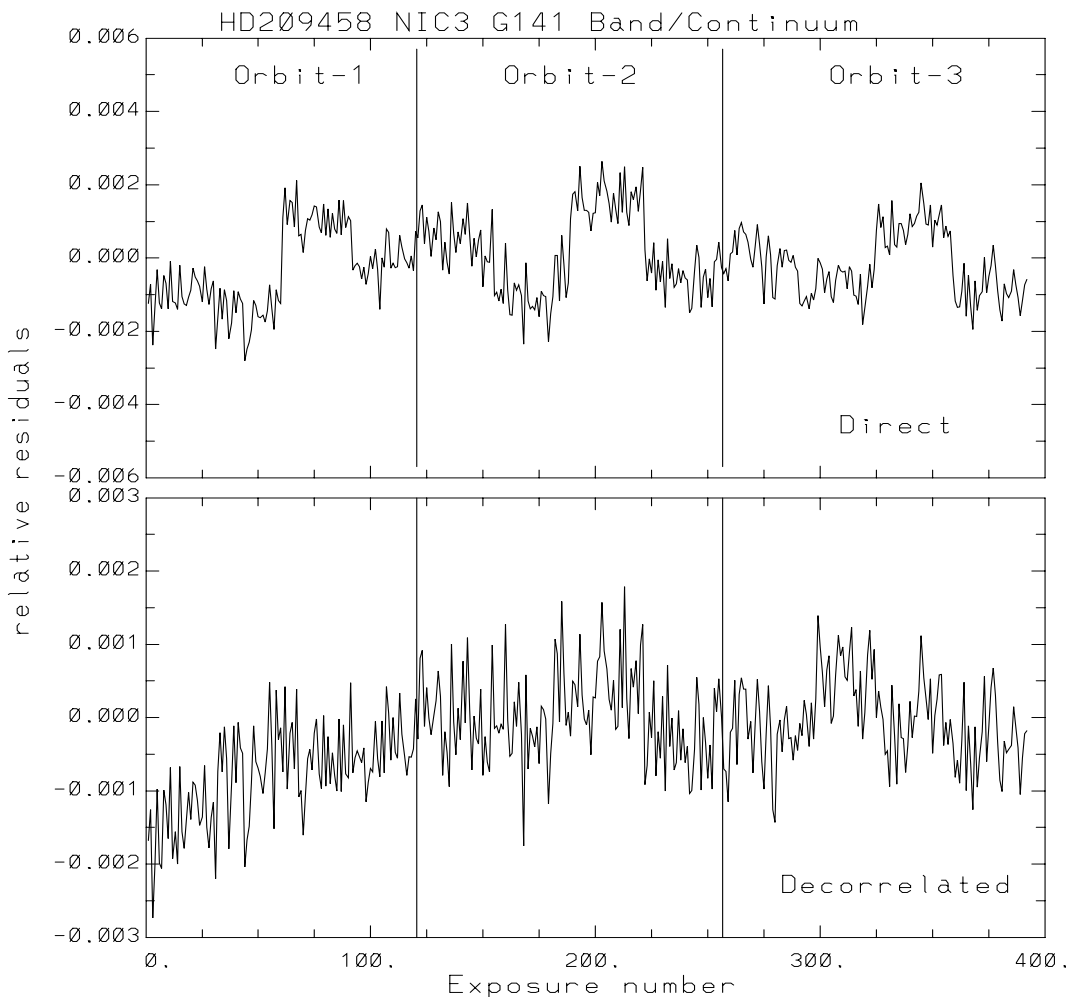


Figure 7- Upper panel shows record (see Fig. 3) of the central Band sum normalized to sum of the two continuum bands to create a differential measure in wavelength. Minus the mean, divided by the mean. The lower panel shows the same after decorrelation with the eight vectors.

High Signal-to-Noise, Differential NICMOS Spectrophotometry

Here the Poisson limited point-to-point S/N is almost exactly 2,000. In the lower panel this is shown after decorrelation with all eight auxiliary parameter vectors, the S/N reached is about 1,700. Therefore for this more differential measurement, as might well be expected, the point-to-point results are closer to the Poisson limit than were the full sum time series.

The more relevant test on these data is to assess how stable the results are orbit-to-orbit after averaging over the central 128 data points of orbits 2 and 3 separately. Relative to the point-to-point rms limits we could hope for a gain of $\sqrt{128} = 11.3$ (or factor of $\sqrt{2}$) less than this for how close to unity the ratio of these two means should be. Summed over single orbits the number of electrons in the central band are 8.80×10^8 and in the two neighboring continua 1.62×10^9 . This implies an orbit-to-orbit Poisson limit a little better than 20,000 or fluctuations of 5×10^{-5} . The orbit 2 mean relative to orbit 3 mean comes out to be 1.00002, i.e. better than the assumed Poisson limit. Of course if the data really are performing near the Poisson limit and we've reduced the comparison to only two numbers its not unreasonable by chance to be better than one-sigma. However, it is also a signal for caution in interpreting the strength of the conclusion.

Another statistic to check as regards the NICMOS stability for measuring orbit-to-orbit changes in the band/continuum ratio is simply to note the differences in the upper panel of Figure 7. In this case the ratio of orbit 2 to orbit 3 means is 1.0003 -- this is before applying any decorrelation corrections. This, by a factor of a few, is not at the Poisson limit, but it is still quite impressive that the orbit-to-orbit means for the spectrophotometric differential differ by only 3×10^{-4} .

Now we return to the caution which ended the next to last paragraph. Decorrelation is a safe step when a sufficiently large number of degrees of freedom exist in the signal compared to the parameters being regressed against. With a total of 256 data points in orbits 2 and 3 for the regression and only eight decorrelation vectors there is no danger of over-correcting the data for high frequency variations. However, consider a case where the signal of interest is just the two numbers of orbit to orbit means, and one of the auxiliary parameters just happens to be dominated by an orbit-to-orbit difference. Even though there may be no causal connection between the orbit-to-orbit offset in the auxiliary parameter and any similar orbit-to-orbit offset in the signal, a decorrelation will perfectly remove the signal changes across orbits. Examination of the auxiliary parameters in Figs 5a and 5b shows that one in particular, the spectrum rotation of Panel C shows a predominant offset between orbits 2 and 3. Dropping this vector from the multi-linear regression, however, still results in the orbit-to-orbit comparison being better than the nominal Poisson limit.

Summary

Time series spectrophotometry with NICMOS using the G141 grism on a bright star has demonstrated S/N of 2,000 for 1.8 second integrations. Likewise the time series for a differential comparison of a central 0.2 micron bandpass sum compared to two comparably large neighboring continuum regions shows a point-to-point S/N of 1,700. In this experiment 136 of these exposures were obtained per orbit, and we have compared sums of the central 128 of these orbit-to-orbit. For the differential spectrophotometric comparison, without applying any further time series cleaning, the direct orbit-to-orbit means differ only at the level of 3×10^{-4} . Applying decorrelation with several auxiliary parameters improves this orbit-to-orbit comparison by more than a factor of 10, in fact to a level better than Poisson.

Having argued on the one hand that the NICMOS stability comparison is quite good, and on the other hand that part of this analysis poses the distinct danger of over-correcting the data, what can be concluded? The primary goal of this test was to compare the orbit to orbit stability of a differential bandpass ratio; here the direct result, obtained without concern of overcorrection came out to be an impressive 3×10^{-4} . It is certainly the case that with more extensive data acquisition as would likely follow in any science application, the existence of several independent orbits of data would enable some degree of decorrelation for orbit to orbit behavior.

Importantly, no particular limitations to reaching quite high signal-to-noise levels for differential spectrophotometry orbit-to-orbit were encountered. It seems reasonable to assume that such measurements in well planned observations can be pushed to near the 10^{-4} level, if not better, assuming of course the existence of adequate count levels.

We thank Eddie Bergeron for evaluating a temperature record for NIC3 based on the bias-level analysis technique. We thank Sangeeta Malhotra and Rodger Thompson for discussion in the planning stages.

References

- Charbonneau, D., et al. 2002, ApJ, 568, 377
Gilliland R.L. 1999, STIS ISR 99-05
Gilliland, R.L., Goudfrooij, P., & Kimble, R.A. 1999, PASP, 111, 1009
Robinson, et al. 1995, PASP, 107, 1094